CHINESE JOURNAL OF PHYSICS VOL. 48, NO. 6 DECEMBER 2010

Coherent Long-distance Signal Detection Using Stimulated Emission: a Feasibility Study

Thilo Dellwig,[1] Matthew R. Foreman,[2] and Fu-Jen Kao[1,*]

[1]*Institute of Biophotonics, National Yang-Ming University, Taipei 11221, Taiwan*
[2]*Blackett Laboratory, Imperial College London, Prince Consort Road, London, SW7 2BZ, United Kingdom*

(Received November 23, 2010)

Stimulated emission based imaging techniques, especially stimulated emission microscopy, are well established and well documented techniques in the realm of biomedical applications. The utilization of a stimulated emission signal offers a variety of advantages over classical linear optical imaging, especially for the identification of biological specimens with high spatial resolution in three dimensions. There is, however, one aspect of the inherent properties of stimulated emission that so far has not received much attention and has not been utilized to its full potential. This aspect, namely the spatial coherence of the stimulated emission signal with the incoming stimulation light, can be utilized for long-distance signal detection of biomedical specimens. The feasibility of this approach is presented here.

PACS numbers: 42.79.Pw, 78.45.+h, 87.57.-s

I. INTRODUCTION

Fluorescence (or spontaneous emission), as well as stimulated emission, are widely used in optical imaging for biomedical applications (see, e.g., [1–13]). For example, a large number of imaging setups are based upon confocal microscopes and advanced light sources. Usually laser-based, these light sources are focused on or into a sample in order to achieve the maximum spatial resolution [14]. Stimulated emission is often utilized in preference to fluorescence due to the higher attainable signal power [15], the better spatial resolution afforded by the non-linear response [16], and the temporal resolution achievable when using ultra-fast lasers [8]. Such microscopy based imaging methods, however, have not to date exploited the intrinsic spatial coherence of the stimulated emission signal with the incoming stimulation light. In turn such methods suffer from limited working distances and small fields of view.

To illustrate this point, consider Fig. 1 which schematically compares the forward direction radiation pattern for different experimental setups. Specifically Fig. 1(a) considers spontaneous emission (red) from a sample, when excited by a collimated illumination (blue). Note the same emission geometry would result for a focused excitation beam. Fig. 1(b) instead considers stimulated emission (orange) when a collimated pump and focused stimulation beam (green) are employed. A broad spatial distribution is seen in both cases, albeit the spread arises in the former case due to the random nature of emission, whilst in the latter it occurs due to the coherence between the stimulation and emitted light. Practically short working distances and small fields of view result for these configurations due to the necessity to maximize the fraction of light collected by subsequent detection optics, whilst

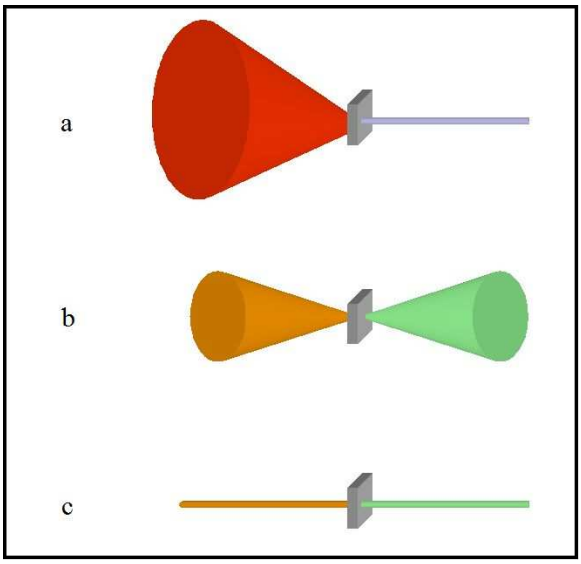

FIG. 1: Comparison of typical spatial distributions in the forward direction of (a) fluorescence, (b) emission stimulated by a focused beam, and (c) emission stimulated by a collimated laser beam. The light travels from right to left, for (b) and (c) the collimated excitation beam is not shown. Color coding: blue: collimated excitation beam; red: fluorescence; green: stimulation beam; orange: stimulated emission.

minimizing cross contamination between neighboring voxels. Additionally a focused illumination configuration will realistically give rise to both fluorescence and stimulated emission signals, which significantly overlap spatially, hence limiting the possibility to distinguish both signals by either spatial or temporal filtering, even when using an ultra-short pulsed laser.

Fig. 1(c) however considers the radiation pattern for stimulated emission from a sample when both stimulation and excitation beams are collimated. Due to the coherent nature of stimulated emission, the spatial distribution of the emitted signal again reflects that of the stimulation beam and hence a tightly distributed emitted beam results. Accordingly the relative distance between sample and detector has minimal influence on the signal strength, allowing long-range detection. Background fluorescence is again unavoidable with this experimental configuration. However, the resulting large angular spread (see Fig. 1(a)) allows it to be significantly suppressed in comparison to the simulated emission signal, via spatial filtering. It should be noted that when using collimated beam geometry the system resolution is determined by the diameter of the excitation or stimulation beam (whichever is smaller). Use of a focused excitation beam, for example, allows high resolution imaging, whilst also preserving the tight angular distribution of the emitted beam. However, it would require the illumination optics to be located close to the sample (detection optics can nonetheless be placed at greater distances).

The collimated configuration itself also does not provide any axial resolution along the beam path. There are however ways to re-gain axial resolution without the need for

focusing, and hence enable full three-dimensional imaging. For example, computer aided tomography can be used. By rotating the sample and recording the obtained signals, a three dimensional image can be reconstructed in a similar manner to X-ray computer tomography.

In this article we present a proof-of-principle via the long-range detection and imaging of stimulated light emission from moieties. Such long-range detection could, for example, potentially be of use in image-guided surgery [17] or airborne (or perhaps ultimately satellite) biological and environmental monitoring [18]. The experimental setup is first described in Section II, before long-range experimental images are given in Section III. As opposed to microscopy applications, the field-of-view imaged is relatively large (in the range of 10 mm by 10 mm), whilst imaging or working distances, i.e., the distance between the sample and the detection device, of up to 2 m are demonstrated. The imaging distance is seen to be limited only by the divergence of the laser beams. Output signal characteristics using a collimated stimulation and excitation beam configuration can differ to microscopy based imaging techniques, since interaction volumes can be significantly larger. Section IV, hence proceeds to establish the output characteristics. Both experimental data and a preliminary theoretical model are given. Finally a short discussion is provided in Section V.

II. EXPERIMENTAL SETUP

The experimental setup used is depicted schematically in Fig. 2. A transmission geometry is adopted as frequently used in in vitro studies. The excitation beam light source is a 532 nm continuous wave (cw) TEM_{00} diode laser with linear polarisation. To enable the use of a lock-in amplifier, the beam intensity is sinusoidally modulated at a frequency of 36 KHz. The typical average laser power on the sample is between 10 to 20 mW. The stimulation beam with a wavelength of 570 nm is produced from a photonic crystal fiber (PCF) with appropriate filters by coupling a mode-locked Ti:Sa ultra-short pulse laser, producing 200 fs pulses at a repetition rate of 76 MHz and a wavelength of 800 nm. For the experiments described the stimulation beam is also linearly polarised, albeit perpendicular to the excitation beam, allowing for better noise suppression with regard to stray light and reflections induced by the excitation beam. Whilst when studying anisotropic and ordered samples perpendicularly polarised excitation and stimulation beams lead to low stimulation efficiencies, this is not an issue in our experiments since our samples constitute an ensemble of randomly oriented fluorescent molecules.

The excitation and stimulation beam are coupled collinearly using a beam splitter and fed into a commercially available microscope scan unit, from which all imaging optics except the x- and y- scanning galvanometers were removed. Between the scan unit and the sample position a single plano-convex collimation lens with a focal length of 400 mm is placed. The long focal length is chosen to mitigate the astigmatism introduced by the fact that the x- and y-scanning mirrors do not rotate around the same focus point. Since a focus shift is, however, introduced by the collimation lens, both excitation and stimulation beams are initially passed through pre-compensation optics before coupling into the scan unit. The back-reflecting mirror behind the sample is a dichroic short-pass mirror, reflecting only

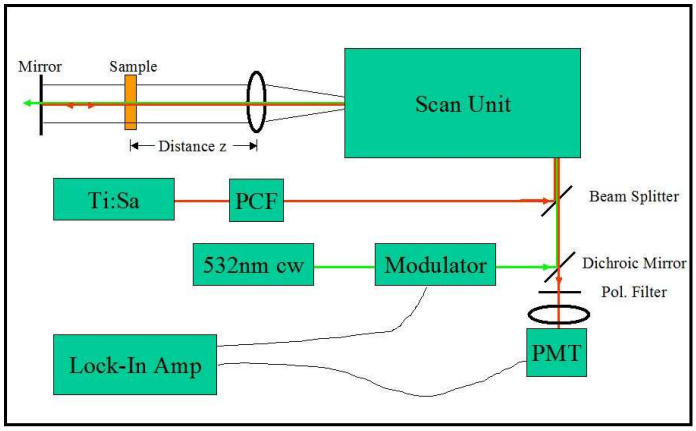

FIG. 2: Experimental setup. The excitation beam (532 nm) and the stimulation beam (570 nm after PCF) are combined and directed onto the sample via a scan unit. The stimulated emission signal is back-reflected through the sample and the scan unit and directed on to the PMT. The distance z can be varied between 1 cm and 200 cm.

wavelengths above 540 nm and therefore eliminating secondary excitation of the sample. It is aligned in a way that the reflected stimulation beam is collinear with the incoming beams, while traveling in the opposite direction.

The detection system consists of: a dichroic beamsplitter, decoupling the reflected signal beam from the light path of the excitation beam; a polarisation filter; a dichroic long-pass filter for further suppression of the excitation wavelength; a focusing lens and a photomultiplier tube (PMT) operated in a linear response mode. The PMT signal is coupled into a lock-in amplifier synchronized with the excitation beam modulator in frequency and phase. The advantage of this optical setup is that the beams pass the galvanometer scanner mirrors twice in opposite directions, therefore self-compensating the x- and y-modulations of the beams' propagation angles (save for the astigmatism mentioned above and beam divergence effects). A spatially static signal on the PMT entrance window is hence produced.

The optical setup, specifically for the wavelengths utilized, was optimized for the detection of Rhodamine 6G as the sample dye. This particular dye was considered due to its prevalence in biomedical investigations. Rhodamine 6G absorbs light in a broad spectrum around 550 nm and has a peak fluorescence wavelength of 570 nm [19]. Samples used were produced using microscope quartz cover glasses, either containing dissolved Rhodamine 6G between two stacked cover glasses, or individual cover glasses marked with a commercially available fluorescent marker pen containing Rhodamine 6G as fluorescent dye. Whilst the Rhodamine concentration of the marker pen is not known and the thickness of the marking varies across the field of view, hence hampering detailed analysis, relative measurements allow the viability of long-range detection to be demonstrated. Full quantitative measurements are ongoing and will be published in a subsequent article.

III. LONG DISTANCE STIMULATED EMISSION IMAGING

The first experiment conducted demonstrates the feasibility of using the described optical setup for long-distance stimulated emission imaging. The sample used was a stack of two quartz glass plates with a random distribution of Rhodamine 6G in between. Imaging was performed with a field of view of 10 mm by 10 mm and a resolution of 256×256 pixels. Notably, the distance of the sample from the collimating lens was 50 mm. Fig. 3(a) shows the images obtained.

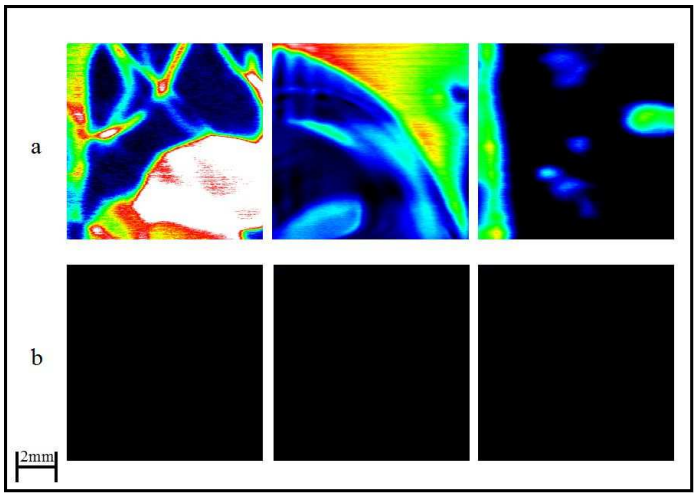

FIG. 3: Stimulated emission (a) and fluorescence (b) images of samples of random Rhodamine 6G distributions. Note that no fluorescence signal is detected.

Spatial filtering to suppress the background fluorescence signal is achieved naturally due to the finite size of the PMT window and since the incident fluorescent power falls as the square of the distance from the source. For example, in moving from a typical working distance of 0.5 mm in microscopy to the 50 mm used here, a suppression of the fluorescence signal of some four orders of magnitude would be expected. Such a decrease is not expected for stimulated emission signal due to the tight distribution of the beam. To verify this suppression in our experiment, imaging was repeated with a beam block placed in the path of the stimulated emission beam. Fig. 3(b) shows the acquired images in this case for the different samples, in which the measured signal was consistently within the noise range of the PMT. The measured signal in Fig. 3(a) hence stems purely from stimulated emission and not from fluorescence of the sample as expected.

Furthermore the feasibility of stimulated emission imaging over larger distances was also verified. In this case the sample comprised a single cover glass marked with a fluorescent marker pen as described above. Fig. 4 shows the acquired images at working distances of (a) 15 cm and (b) 2 m from the collimation lens. Reference images detecting purely the fluorescence were again taken, but have been omitted here as they show negligible signal. From Fig. 3 it is evident that the sample structure is reproduced well, even at large distances,

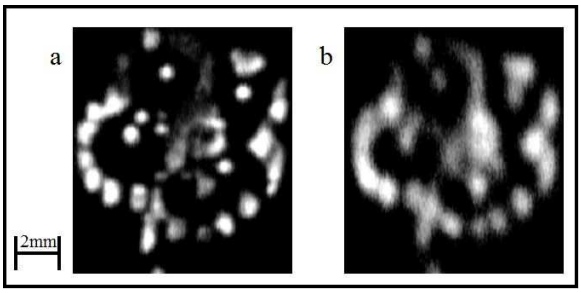

FIG. 4: Stimulated emission images of a sample produced using a fluorescent marker pen taken at a distance of (a) 15 cm and (b) 200 cm away from the collimation lens.

hence demonstrating the viability of long range imaging. However, the degradation in the image resolution is seen at greater distances.

The lasers used in the experiment have a divergence of approximately 1.7 mrad. Immediately after the collimation lens, the beam diameter of the stimulation beam is ∼0.3 mm, which in turn determines the resolution limit of the imaging system. Using the definition

$$\text{Divergence} = 2\arctan\left[\frac{d_\text{f} - d_\text{n}}{2l}\right]$$

with the distance l, the beam diameter at the far position d_f and the beam diameter at the near position d_n, the beam diameter at the 2 m position calculates to 3.7 mm. The resolution loss seen is hence attributable to the divergence of the laser beams.

IV. EXCITATION AND STIMULATION BEAM POWER CORRELATIONS

Microscopic stimulated emission studies inherently consider signal generation in a relative small interaction volume. In the presented setup, however, excitation and stimulation by means of unfocused beams implies that the interaction volumes can be significantly larger, especially for thick samples. The characteristics of the output signal can hence differ in comparison. In order to characterize the optical system, a number of measurements with varied beam powers were therefore conducted. Samples comprised single cover glasses marked with a fluorescent marker pen as described above and a working distance of 50 mm was used, whilst other setup details were identical to those used previously. Fluorescence images were again collected and found to lie within the PMT noise.

In a first experiment, the stimulation beam power was kept constant at 35 nW and the excitation power varied between 9.6 mW and 18 mW. As can be seen in Fig. 5, the brightness of the obtained images varies accordingly. Using image analysis software, several different locations on the images were selected and the varying grey level data read out. Fig. 6 shows the brightness, i.e., the stimulated emission response of these locations as a function of the excitation beam power. It can clearly be seen that the stimulated emission signal rises with increasing power of the excitation beam until a saturation of the signal

strength is reached. Note that the relative increase of signal strength compared to that of the excitation beam is, within error margins, the same for all locations. This indicates that the excitation beam energy is not fully absorbed by the sample and the stimulated emission signal strength is limited by the number of Rhodamine 6G molecules that can be transferred into an excited state. This is to be expected for such thin dye layers.

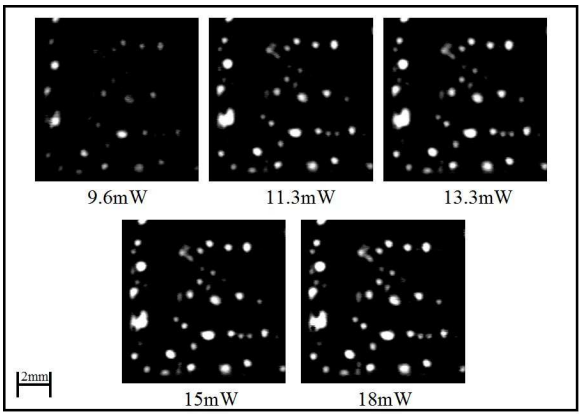

FIG. 5: Images of a sample produced with a fluorescent marker pen for different excitation beam powers.

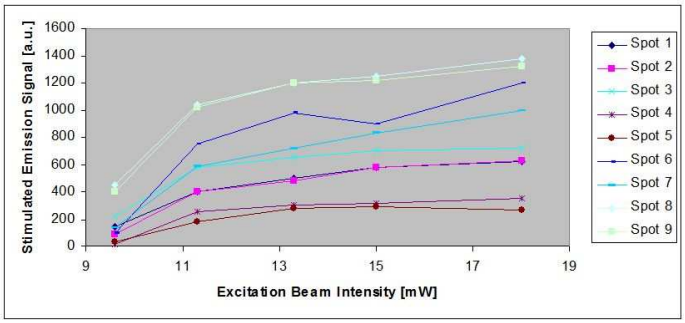

FIG. 6: Dependence of the stimulated emission signal strength on the excitation beam power, for a number of locations of the sample depicted in Fig. 4.

In a similar experiment, the excitation beam power was kept constant at 20 mW and the stimulation beam power varied between 13 nW and 40 nW. Fig. 7 shows the stimulated emission signal versus the stimulation beam power for several locations. Again, the stimulated emission signal increases with the stimulation beam power until saturation is reached. In this case, however, the relative power change decreases with increasing absolute stimulated emission power, i.e., the signal from thicker rhodamine 6G layers saturates faster.

In order to understand this saturation behaviour, the qualitative model described below was considered. It is noted that this qualitative model does not consider the full

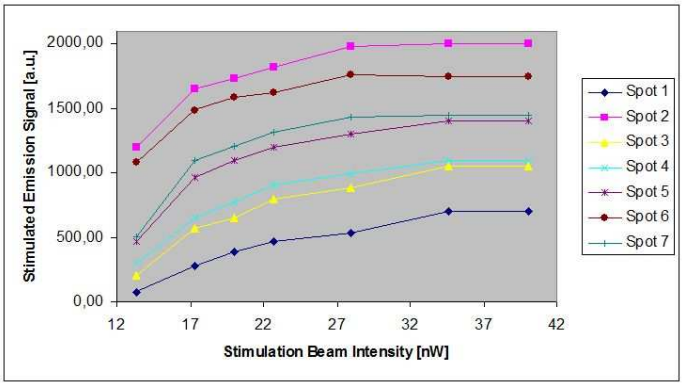

FIG. 7: Dependence of the stimulated emission signal strength on the stimulation beam power for a number of locations of a sample produced using a fluorescent marker pen.

experimental details, such as the lock-in amplification and pulsed stimulation, however it is believed to incorporate the pertinent underlying physical processes, as corroborated by agreement with experiment. A more detailed theoretical explanation will again be the topic of a later publication.

Consider then the propagation of a light beam with spectral intensity $I(\omega, z)$ in the z-direction of a medium (the unfocused stimulation beam). A two level model is used to describe the energy structure of the molecules in the medium, such that the change in spectral intensity after propagating a distance dz is given by [20]

$$[I(\omega, z + dz) - I(\omega, z)]\, A d\omega = (N_2 B_{21} - N_1 B_{12}) \phi(\omega) g(\omega - \omega_0) A dz \hbar\omega d\omega, \tag{1}$$

where the subscripts 1 and 2 denote the ground and excited states with population densities of N_1 and N_2 respectively, $\phi(\omega)/c$ is the spectral energy density, $g(\omega - \omega_0)$ is the normalized lineshape function, B_{21} and B_{12} are the Einstein coefficients, A is the area of the beam cross-section, and c is the speed of light.

This equation can also be expressed, in the limit $dz \to 0$, as

$$\frac{\partial I(\omega, z)}{\partial z} = \alpha(\omega - \omega_0) I(\omega, z) \tag{2}$$

with the gain coefficient

$$\alpha(\omega - \omega_0) = (N_2 B_{21} - N_1 B_{12}) \hbar\omega \frac{g(\omega - \omega_0)}{c}. \tag{3}$$

Also introducing the excitation rates, R_2 and R_1, for the excited state and the ground state respectively, the rate equations for N_1 and N_2 are [20]:

$$\frac{dN_2}{dt} = R_2 - (N_2 B_{21} - N_1 B_{12}) \int \phi(\omega) g(\omega - \omega_0) d\omega - \frac{N_2}{\tau_2}, \tag{4}$$

$$\frac{dN_1}{dt} = R_1 + (N_2 B_{21} - N_1 B_{12}) \int \phi(\omega) g(\omega - \omega_0) d\omega - \frac{N_1}{\tau_1} + N_2 A_{21}, \tag{5}$$

where the terms N_i/τ_i describe decay processes and the term $N_2 A_{21}$ describes spontaneous emission.

Neglecting the pulsed nature of the stimulation beam, and noting that the lock-in modulation frequency is low compared to other processes, a steady state is assumed such that $dN_2/dt = dN_1/dt = 0$. Furthermore narrow band radiation of frequency ω_L can also be assumed due to spectral filtering present in the optical setup. From Equation (3), it then follows that

$$\alpha(\omega - \omega_0) = \frac{\alpha_0(\omega_L - \omega_0)}{1 + I(\omega_L)/I_\mathrm{s}}, \tag{6}$$

where $\alpha_0 = [R_2\tau_2 B_{21} - (R_1\tau_1 + R_2\tau_2 A_{21})B_{12}]\hbar\omega g(\omega_L - \omega_0)/c$ is the small signal gain coefficient and $I_\mathrm{s}^{-1} = [\tau_2 B_{21} + (\tau_1 - A_{21}\tau_2)B_{12}]g(\omega_L - \omega_0)/c$ is the (constant) saturation power.

The power dependent gain coefficient α can be used to calculate the signal strengths for the stimulation beam passing through a thick Rhodamine 6G sample in the z-direction via the differential equation.

$$\frac{\partial I}{\partial z} = \alpha I. \tag{7}$$

Substituting from equation (6) and integrating from $z = 0$ to $z = d$, finally yields

$$\ln\left[\frac{I(d)}{I(0)}\right] + \frac{I(d) - I(0)}{I_s} = \alpha_0 d. \tag{8}$$

There are two interesting limiting cases for equation (8). The first one describes the behaviour for small powers, i.e., $I(d) \ll I_\mathrm{s}$. Equation (7) can then be approximated by $\partial I/\partial z \approx \alpha_0 I$, which leads to the solution

$$I_\mathrm{small}(d) = I(0)e^{\alpha_0 d}. \tag{9}$$

The second interesting case is when $I(d)$ comes close to the saturation intensity, i.e., $I(d) \approx I_\mathrm{s}$. As typical gains for stimulated emission are in the range of 10^{-7} [21], the logarithmic portion of Equation (8) can be neglected relative to the linear term, hence

$$I_\mathrm{large}(d) = I(0) + \alpha_0 I_\mathrm{s} d. \tag{10}$$

This behaviour also governs the regime $I(d) \gg I_\mathrm{s}$, as $1 + I(d)/I_\mathrm{s} \approx I(d)/I_\mathrm{s}$ for this case.

The ratio between the output intensity at saturation and the output intensity for small input powers hence becomes

$$\frac{I_\mathrm{large}}{I_\mathrm{small}} = \frac{I_\mathrm{large}(0) + \alpha_0 I_\mathrm{s} d}{I_\mathrm{small}(0)e^{\alpha_0 d}}. \tag{11}$$

In order to compare the experimental data with the model derived above, a number of boundary conditions of the experiment have to be taken into account. As the thickness, d, and concentration (influencing the power gain α) of the dye on the samples has not been measured, the relative thicknesses of the individual measurement location (in arbitrary units) have to be estimated from the measured output powers. As the lateral beam interaction areas remain constant throughout the experiments, the output power is proportional to the output intensity $I(d)$ and hence equations (9) and (10) can be used for this estimation. Fig. 8(a) depicts the calculation of the quantity $\alpha_0 d$ versus the measured powers for each location as found using equation (9) (circles) and equation (10) triangles. The parameter I_s was numerically determined to obtain best consistency across all available data points. As expected, the two curves diverge for extreme values and yield relatively similar results for medium values.

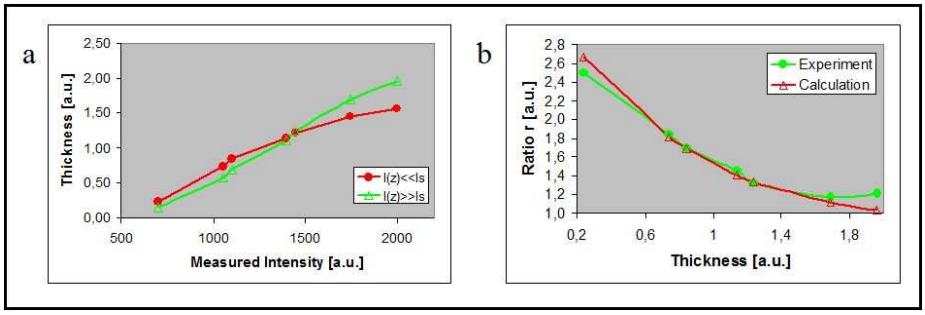

FIG. 8: (a) Relative thickness of the sample locations calculated using the experimental results and equation (9) (circles) and equation (10) (triangles) respectively; (b) Comparison of the experimental results (circles) and calculated values according to equation (11) (triangles) for the measured power ratio.

Using the $\alpha_0 d$-values from the $I(d) \ll I_s$ curve for low power values (i.e., for signals below the intersection at 1400 a.u. of the plots of Fig. 8(a)) and $\alpha_0 d$-values from the $I(d) \gg I_s$ curve for high power values ($>$ 1400 a.u.), the intensity ratios according to equation (11) can now be calculated and compared to the experimental results. Both these curves are shown in Fig. 8(b).

The conclusion from the good fit of both curves is, that the model presented is valid. Physically the model implies that photons created by the incoming stimulation beam can themselves stimulate additional photon emission along the remaining light path and therefore lead to a faster saturation of the gain for thicker samples.

V. SUMMARY AND OUTLOOK

In this article we have shown how the spatial coherence properties between the stimulation and emitted beam in stimulated emission imaging can be exploited to allow long working distances and large fields of view. Specifically the tight angular distribution of

an unfocused stimulation beam is inherited by the emitted beam, which furthermore was shown to allow significant suppression of background fluorescence by means of spatial filtering. Working distances of up to 2 m were demonstrated, where laboratory dimension were the only obstacle to verifying the principle at larger distances.

The resolution of imaging was seen to depend on the size of either the stimulation or excitation beam, in addition to the detection distance. Whilst the former need not be of consequence in experimental arrangements where short range illumination can be used, it does however present a drawback if both long-range detection and illumination are desired. Data regarding the resolution degradation with increasing working distance was consistent with that resulting from beam divergence alone.

Dependencies between the measured signal power and the excitation and stimulation beam powers have also been presented. Such considerations can prove to be of importance due to saturation effects that can arise in comparison to existing stimulated emission microscopy techniques in which interaction volumes are intrinsically small. A preliminary model describing the emitted signal dependence, and gain saturation, of the stimulation beam has been presented and verified qualitatively using experimental data. A fuller quantitative verification of this model will however be the subject of a later publication.

In closing it is worthwhile to note that spatial coherence and directionality are inherent in many other non-linear processes such as Coherent Anti-Stokes Raman Spectroscopy(CARS), and harmonic generation. Long distance detection is therefore conceivable in a larger domain of non-linear imaging and sensing than that presented here.

Acknowledgement

The authors would like to thank the National Science Council, Taiwan (NSC99-2627-M-010-002-, NSC98-2627-M-010-006-, NSC97-2112-M-010-002-MY3, and NSC98-2112-M-010-001-MY3), as well as the Ministry of Education, Taiwan under the "Aim for Top University" project for the generous support of the reported work.

References

* Electronic address: fjkao@ym.edu.tw

[1] V. Ghukasyan and F.-J. Kao, J. of Phys. Chem. C **113**, 11532–11540 (2009).
[2] F.-J. Kao, Micro. Res. and Tech. **63**, 175–181 (2004).
[3] V. Ghukasyan, C. C. Hsu, C. R. Liu, F.-J. Kao, and T. H. Cheng, J. Biomed. Opt. **15**, 016008 (2010).
[4] S. W. Hell and J. Wichmann, Opt. Lett. **19**, 780–782 (1994).
[5] Y. Garini, B. J. Vermolen, and I. T. Young, Curr. Opin. Biotechnol. **16**, 3–12 (2005).
[6] E. M. Hillman, J. Biomed. Opt. **12**, 051402 (2007).
[7] S. Jakobs, BBA **1763**, 561–575 (2006).
[8] K. Dowling *et al.*, Opt. Lett. **23**, 810–812 (1998).
[9] K. Isobe *et al.*, Opt. Express **14**, 786–793 (2006).

[10] S. Deng, L. Liu, Y. Cheng, R. Li, and Z. Xu, Opt. Express **18**, 1657–1666 (2010).
[11] G. Moneron and S.W. Hell, Opt. Express **17**, 14567–14573 (2009).
[12] B. R. Rankin and S. W. Hell, Opt. Express **17**, 15679–15684 (2009).
[13] J. J. Field *et al.*, Opt. Express **18**, 13661–13672 (2010).
[14] S. Hell and E. H. K. Stelzer, J. Opt. Soc. Am. A **9**, 2159–2166 (1992).
[15] C. E. Hamilton, J .L. Kinsey, and R. W. Field, Ann. Rev. Phys. Chem. **37**, 493–524 (1986).
[16] W. Denk, J. H. Strickler, and W .W. Webb, Science **248**, 73–76 (1990).
[17] A. M. De Grand and J. V. Frangioni, Technol. Cancer Res. Treat. **6**, 553–562 (2003).
[18] M. A. Sundermeyer *et al.*, J. Atmos. Oceanic Technol. **24**, 1050–1065 (2007).
[19] A. Penzkofer, W. Leupacher, and J. Luminisc. **37**, 61–72 (1987).
[20] B. A. E. Saleh, M. C. Teich, *Fundamentals of photonics, 2nd edition*, (Wiley-Interscience, 2007).
[21] M. Wei *et al.*, Nature **461**, 1105–1109 (2009).